

# Performance Evaluation of Real-time and Scale-invariant LoG Operators for Text Detection

Dinh Cong Nguyen<sup>1,2</sup>, Mathieu Delalandre<sup>1</sup>, Donatello Conte<sup>1</sup> and The Anh Pham<sup>2</sup>

<sup>1</sup>Tours University, Tours City, France

<sup>2</sup>Hong Duc University, Thanh Hoa, Vietnam

{mathieu.delalandre, donatello.conte}@univ-tours.fr;

{nguyendinhcong, phamtheanh}@hdu.edu.vn

**Keywords:** Text detection, LoG, blobs, key-points, real-time, estimators, DoG, fast Gaussian filtering, scale-space, stroke model, groundtruthing, performance characterization, repeatability.

**Abstract:** This paper presents a state-of-the-art and a performance evaluation of real-time text detection methods, having particular focus on the family of Laplacian of Gaussian (LoG) operators with scale-invariance. The computational complexity of operators is discussed and an adaptation to text detection is obtained through the scale-space representation. In addition, a groundtruthing process and a characterization protocol are proposed, performance evaluation is driven with repeatability and processing time. The evaluation highlights a near-exact approximation with real-time operators at one to two orders of magnitude of execution time. The real-time operators are adapted to recent camera devices to process high resolution images. Perspectives are provided for operator robustness, optimization and characterization of the detection strategy.

## 1 INTRODUCTION

Text processing in natural images is a core topic in the fields of image processing and pattern recognition. Recent state-of-the-arts on methods and international contests can be found in (Ye and Doermann, 2015) and (Gomez et al., 2017), respectively. A key problem is to make these methods being time efficient so that they can be embedded into devices (e.g. smartphone, tablet, smart camera) to support a real-time processing (Yang et al., 2015; Girones and Julia, 2017; Deshpande and Shriram, 2016).

The real-time systems in the literature (Gomez and Karatzas, 2014; Liu et al., 2014; Yang et al., 2015; Girones and Julia, 2017) apply the strategy of two stages composing of detection and recognition. The detection stage localizes the text components at a low complexity level and groups them into text candidate regions before classification. The goal is to get a perfect recall for the detection with a maximum precision for optimization of the recognition. The two-stage strategy differs from the end-to-end strategy, that applies a direct template/feature matching with classification using high-level models for text (Neumann and Matas, 2016).

The text elements in natural images present specific shapes with elongation, orientation and stroke

width variation, etc. as shown in Figure 1. This makes difficult to the detection problem. Hence, various approaches have been investigated in the literature to design real-time and robust methods.

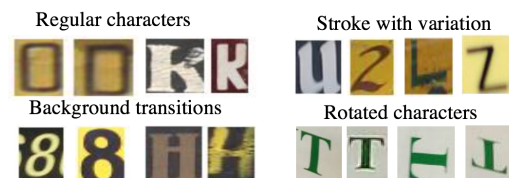


Figure 1: Example of text elements/characters in images, extracted from (de Campos et al., 2009).

The published works drive the text processing as a blob detection problem with the maximally stable extremal regions (MSER) (Yang et al., 2015; Deshpande and Shriram, 2016) and the LoG-based operators (Liu et al., 2014; Girones and Julia, 2017).

MSER looks for the local intensity extrema and applies a watershed-like segmentation algorithm. The operator is rotation, scale and affine-invariant. It can be processed at a linear complexity (Salahat and Qasaimeh, 2017). It performs well with background/foreground regions but is sensitive to blurring.

Alternative to MSER is the Laplacian of Gaussian (LoG) operator. The LoG operator is also a blob de-

Symbols	Meaning	Symbols	Meaning
Continuous/discrete domain		$\nabla^2$	Laplacian
$f$	An image function/raster	$\hat{\phantom{x}}$	Estimator
$g$	A Gaussian function/operator	$k$	Parameter to control approximation between LoG, DoG
$\Pi$	A step function/box filter	$\mathfrak{O}$	The stroke model function $\sigma_s = \mathfrak{O}(w)$
$w$	Stroke width parameter with $w \in [w_{min}, w_{max}]$	Discrete domain	
$a$	Signal amplitude	$\lambda$	Weighting parameter
$\beta, \alpha$	Thresholding parameters	$\omega^2$	Size of operator (width $\times$ height)
$\otimes$	The global convolution product	$(\sigma_0 \dots \sigma_m)$	A filter bank including $(m+1)$ discrete filters
Continuous domain		$n$	Number of box filters
$\sigma, \sigma_s$	The standard deviation, optimum scale for stroke detection	$N$	Size of image
$h, h_s, h_e$	Response with the stroke model, $h_s/h_e$ the stroke/edge optimums	$O$	Complexity
$g_{xx}$ (either $y$ )	Second partial derivative of the $g$ function	$r, \epsilon$	Radius of region, overlap error

Table 1: The symbols used in the paper.

tor. Similar to MSER, it can be made rotation, scale and contrast-invariant. However, it is less sensitive to blurring and can be tuned as a stroke detector. As a general trend, the operator ensures a better characterization of text elements.

The LoG operators can be made real-time and competitive with respect to MSER. At the best of our knowledge, the real-time property of LoG operators has been explored only for spatial filtering and scale-invariance. The operators, which are contrast-invariant (Miao et al., 2016) or generalized (Kong et al., 2013), cannot fit with the real-time constraint.

This paper gives a state-of-the-art and a performance evaluation of real-time and scale-invariant LoG operators for text detection. Adaptation to text detection is achieved by the scale-space representation. Performance evaluation analyzes the impact of real-time operators for text detection with their parameters and gives a comparison of time processing.

The organization of the remainder of the paper is as follows. Section 2 gives the state-of-the-art. Then, performance evaluation of operators is discussed in section 3. At last, section 4 will conclude and propose some perspectives. Table 1 provides the meaning of the main symbols used in the paper.

## 2 STATE-OF-THE-ART

### 2.1 Introduction

The LoG operator is defined as the Laplacian of Gaussian, and then derived from the Gaussian function. The Gaussian function, in a multivariate form, is given in Eq. (1) with a vectorial notation.

$$g(p|\mu, \Sigma) = \frac{1}{(2\pi)^{\frac{n}{2}} \sqrt{|\Sigma|}} e^{-\frac{1}{2}(p-\mu)^T \Sigma^{-1} (p-\mu)} \quad (1)$$

In the two dimensional case,  $n = 2$ ,  $p$  is a point and  $\mu$  a mean.  $\Sigma$  is the diagonal covariance matrix with  $\Sigma^{-1}$  the inverse and  $|\Sigma|$  the determinant, where

the  $\sigma_x, \sigma_y$  parameters in  $\Sigma$  are the standard deviations for the dimensions  $x, y$ . Considering  $\sigma_x = \sigma_y = \sigma$ ,  $\mu$  null and a scalar notation, the Gaussian function Eq. (1) becomes Eq. (2).

$$g(x, y, \sigma) = \frac{1}{2\pi\sigma^2} e^{-\frac{x^2+y^2}{2\sigma^2}} \quad (2)$$

The LoG is a compound operator resulting of the Laplacian  $\nabla^2$  of  $g(x, y, \sigma)$  as Eq. (3).

$$\begin{aligned} \nabla^2 g(x, y, \sigma) &= g_{xx}(x, y, \sigma) + g_{yy}(x, y, \sigma) \\ &= \frac{1}{2\pi\sigma^4} \left( \frac{x^2+y^2}{\sigma^2} - 2 \right) e^{-\frac{x^2+y^2}{2\sigma^2}} \end{aligned} \quad (3)$$

The LoG-filtered image  $h(x, y)$  Eq. (4) is obtained by the global convolution  $\otimes$  between the initial image  $f(x, y)$  and the LoG operator  $\nabla^2 g(x, y, \sigma)$ .

$$h(x, y) = \nabla^2 g(x, y, \sigma) \otimes f(x, y) \quad (4)$$

As illustrated in Figure 2, the response of the LoG operator Eq. (4) is dependent on the  $\sigma$  parameter. At a low value, the operator focuses its response to edges that can be detected with zero-crossing. When  $\sigma$  increases, a peak at the blob location appears in the response. Due to noise, the peak is thresholded to get the blob components. The blob centroid is obtained with a non-maximum suppression in the local neighborhood. The corresponding key-point is expressed with the centroid coordinates and a radius having a normal value  $r = \sqrt{2}\sigma$  for a circular blob.

However, this peak value relies on the correlation between  $\sigma$  and the size of the blob, and a wrong scale can result in a missed detection. To deal with this problem, the standard approach is to handle the operator in the scale-space domain with a filter bank  $(\sigma_0, \dots, \sigma_m)$ . This requires a specific approach for optimization to bound the number of filters and to handle them in a time efficient way.

Another constraint is the processing time for filtering. The convolution product of Eq. (4) has a complexity  $O(N\omega^2)$  with  $N$  the image size (in pixels) and  $\omega^2$  the size (width  $\times$  height) of the LoG filter. The

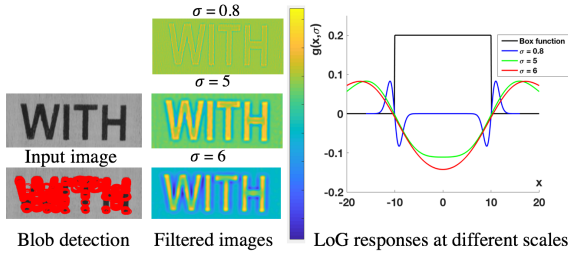


Figure 2: Text detection with a LoG operator with different values for the  $\sigma$  parameter.

size of the filter is dependent on the  $\sigma$  parameter such as we have  $\omega = 6\sigma$  for a full coverage. This leads to a large processing time making the operator little compatible with a real-time use-case. To cope with this problem, several contributions have been proposed in the literature for reformulation and approximation of the LoG operator.

We will discuss the different optimization issues in next sections.

## 2.2 Fast LoG Filtering

The standard approach to accelerate the LoG filtering is to reformulate the LoG function into a Difference of Gaussian (DoG) function and then to approximate the DoG function with a fast Gaussian filtering method.

The DoG function is defined from the heat equation Eq. (5) (Lindeberg, 1994). In Eq. (5), the normalization of the LoG function Eq. (3) with a scale parameter  $\sigma$  gives the derivative of the Gaussian function in the scale-space domain. The left term of Eq. (5) can be reformulated as a local derivative, with  $k$  a parameter and a step offset  $\delta_\sigma = (k-1)\sigma$ . The approximation of the derivative in this equation gets better as  $\delta_\sigma$  goes to 0 when  $k$  comes to 1.

$$\begin{aligned} \sigma \nabla^2 g(x, y, \sigma) &= \frac{\partial g(x, y, \sigma)}{\partial \sigma} \\ &\approx \frac{g(x, y, k\sigma) - g(x, y, \sigma)}{(k-1)\sigma} \end{aligned} \quad (5)$$

With reformulation of Eq. (5), the LoG function can be approximated by mean of a DoG as Eq. (6),

$$\begin{aligned} g(x, y, k\sigma_2) - g(x, y, \sigma_2) &\approx (k-1)\sigma^2 \nabla^2 g(x, y, \sigma) \\ &= \frac{1}{2\pi} \left( \frac{1}{(k\sigma_2)^2} e^{-\frac{x^2+y^2}{2(k\sigma_2)^2}} - \frac{1}{\sigma_2^2} e^{-\frac{x^2+y^2}{2\sigma_2^2}} \right) \end{aligned} \quad (6)$$

with a normalization factor  $(k-1)\sigma^2$ . Considering  $\sigma_1 = k\sigma_2$ , the relation among  $\sigma, \sigma_1, \sigma_2$  is formulated as Eq. (7) (Gonzalez and Woods, 2007).

$$\sigma^2 = \frac{\sigma_1^2 \sigma_2^2}{\sigma_1^2 - \sigma_2^2} \ln \frac{\sigma_1^2}{\sigma_2^2} \quad (7)$$

The DoG function is computed with two Gaussian filters. With convolution, the Gaussian filtering can be implemented in separable way at a complexity  $O(N\omega)$ . When  $\omega$  is large, it is still a time consuming task. Several methods have been proposed in the literature to accelerate the Gaussian filtering and make it independent of the filter size at a complexity  $O(N)$ . These methods attempt to improve computational efficiency in the expense of accuracy. They are referred as fast Gaussian filtering methods. They enter in an estimator cascade methodology where  $LoG \approx DoG \approx \widehat{DoG}$ , with  $\widehat{DoG}$  a DoG estimator.

Survey with performance evaluation can be found in (Charalampidis, 2016; Elboher and Werman, 2012). Two main categories have been investigated including the box and recursive-based filters. The selection of a suitable method depends on the application use-case which is supposed to be solved in term of a good trade-off between speed and accuracy. The Table 2 gives a global comparison of the methods.

Category	Methods	Time optimization	Accuracy
Box filter	Box	++	+++
	SII	+++	++
	KII	+	+
Recursive filter	Deriche	++	++
	TCF	+++	+++
	VYV	+	++

Table 2: Time optimization and accuracy of fast Gaussian filterings: (SII) Stacked Integral Image (VYV) Vliet Young Verbeek (KII) Kernel Integral Image (TCF) Truncated Cosine Functions (+++) best case (+) medium case.

For illustration, we will give here the box filtering method (Kovesi, 2010; Frago et al., 2014). As shown in the Table 2, the method is referred as the top accurate box-based filters and being competitive with the recursive filters. The box filtering method sums up averaging filtering to approximate a Gaussian filter, as Eq. (8) with a desired standard deviation.

$$\widehat{g}(x, y, \sigma) = \sum_{i=1}^n \lambda_i \Pi_i(x, y) \quad (8)$$

In Eq. (8)  $\Pi_i(x, y)$  is a box filter function having a predefined size with a value 1 if  $(x, y)$  are located inside the box, 0 otherwise. The  $\lambda_i$  parameters weight the box filters  $\Pi(x, y)$ .  $n$  is the number of box filters that can be fixed between 4 to 6 for a good trade-off between optimization and robustness (Kovesi, 2010).

From Eq. (8), it becomes possible to approximate the DoG operator by  $\widehat{DoG}$  in Eq. (9) with two sets of box filter functions. As the  $k$  parameter Eq. (5) is supposed to be low<sup>1</sup>, a similar number of filters can

<sup>1</sup>In practice,  $k \in ]1, \sqrt{2}]$ .

be applied for estimation of the two Gaussian kernels.

$$\begin{aligned} \widehat{DoG} &= \widehat{g}(x, y, k\sigma) - \widehat{g}(x, y, \sigma) \\ &= \sum_{i=1}^n \lambda_i \Pi_i(x, y) - \sum_{j=1}^n \lambda_j \Pi_j(x, y) \end{aligned} \quad (9)$$

The DoG-filtered image is achieved by the global convolution Eq. (10) between the input image  $f(x, y)$  and the DoG estimators  $\widehat{DoG}$ .

$$\begin{aligned} &(\widehat{g}(x, y, k\sigma) - \widehat{g}(x, y, \sigma)) \otimes f(x, y) \\ &= \widehat{g}(x, y, k\sigma) \otimes f(x, y) - \widehat{g}(x, y, \sigma) \otimes f(x, y) \\ &= \sum_{i=1}^n \lambda_i \Pi_i(x, y) \otimes f(x, y) - \sum_{j=1}^n \lambda_j \Pi_j(x, y) \otimes f(x, y) \end{aligned} \quad (10)$$

Obviously, the  $\Pi_i(x, y) \otimes f(x, y)$  products of Eq. (10) can be obtained with integral image at a complexity  $O(N)$ . As a result, approximation of the DoG operator could be achieved with  $2n$  accesses to the integral image, it is therefore parameter free.

A core problem with the Gaussian kernel approximation is to fix the  $n$ ,  $\Pi_i(x, y)$ ,  $\lambda_i$  parameters of Eq. (8). The approach used in the literature (Bhatia et al., 2010; Frago et al., 2014) is the minimization of the Mean Square Error (MSE) Eq. (11). This minimization can be achieved by any appropriate numerical methods for regression. In (Fragoso et al., 2014), the LASSO algorithm is used to solve the problem.

$$MSE = \sum_{(x,y) \in [0,w]} (g(x,y) - \widehat{g}(x,y))^2 \quad (11)$$

### 2.3 Scale-space Representation

As discussed in section (2.1), the stroke detection is dependent on the scale parameter  $\sigma$ . To deal with this problem, the standard approach is to deploy a filter bank at different scales ( $\sigma_0, \dots, \sigma_m$ ). This is referred as the scale-space representation in the literature (Lowe, 2004; Nilufar et al., 2012), which is counted on the used operator and the considered detection problem. We will have a particular focus here on the DoG operator for stroke detection.

A time-efficient approach for construction of the scale-space responses with DoG has been proposed in the SIFT descriptor (Lowe, 2004). It was applied in several papers for text detection (Mao et al., 2013; Risnumawan et al., 2014). The approach is illustrated in Figure 3. The input image is convolved with a set of  $(m + 1)$  Gaussian filters having different scales ( $\sigma_0, \dots, \sigma_m$ ). Each scale is fixed as  $\sigma_i = k^i \sigma_0$ . The  $k$  parameter is set to ensure a doubling of  $\sigma_0$  at a  $2^{1/m}$  value. The DoG product is obtained by comparison of adjacent image scales, that reduces by half the needed filters. For optimization purposes, the overall process

is applied with a small set of filters (e.g. 5) and repeated in a closed-loop way, where a re-sampling is used at any loop<sup>2</sup>. The overall computation is then greatly reduced.

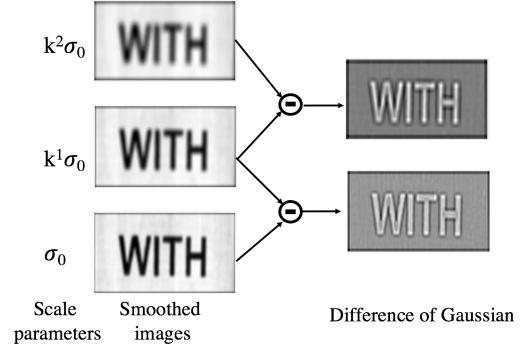


Figure 3: Scale-space representation of (Lowe, 2004).

The approach of (Lowe, 2004) considers an exponential model for the scale-space representation. For stroke detection, contributions in the literature suggest a linear model where the parameter  $\sigma$  is able to be derived from the stroke width parameter  $w$ . This is presented as the stroke model (Liu et al., 2014).

The Figure 4 illustrates the model. The general idea is to look for the convolution response between a LoG-based operator and a stroke signal modeled as a unit step function. We can express then the null cases with the derivatives to get the minimum/maximum of the convolution product. Assuming that these minimum/maximum are located at the center of the stroke  $w/2$ , we can present the standard deviation  $\sigma$  as a function  $\sigma = \mathfrak{O}(w)$ .

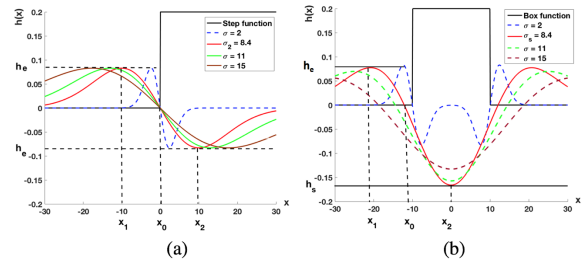


Figure 4: LoG responses at different scales to (a) a step function (b) a boxcar function of size  $w = 21$ .

Assuming the image signal as a function<sup>3</sup>  $a \otimes \Pi(x)$ , where  $\Pi(x)$  is the step function Eq. (12) and  $a$  as the signal amplitude, the convolution product with

<sup>2</sup>Additional optimization is achieved with successive convolutions, we will report the reader to (Lowe, 2004).

<sup>3</sup>For simplification, considering the 1D case.

the LoG operator  $\nabla^2 g(x)$  is given in Eq. (13).

$$\Pi(x_0 - x) = \begin{cases} 0 & x < x_0 \\ 1 & \text{otherwise.} \end{cases} \quad (12)$$

$$\begin{aligned} h(x_0) &= a(\Pi \otimes \nabla^2 g)(x_0) \\ &= a \int_{-\infty}^{+\infty} \Pi(x_0 - x) \nabla^2 g(x) dx \end{aligned} \quad (13)$$

As  $\Pi(x_0 - x)$  is located at  $x_0$ , the convolution product  $\Pi(x_0 - x) \otimes \nabla^2 g(x)$  over  $x$  equals the summation  $\nabla^2 g(x)$  centered at  $x_0$ . With normalization and approximation of  $\nabla^2 g(x)$  as given in Eq. (6), the Eq. (13) is reformulated into Eq. (14).

$$\begin{aligned} (k-1)\sigma^2 h(x_0) \\ \approx \int_{-\infty}^{+\infty} a(g(x_0 - x, \sigma_1) - g(x_0 - x, \sigma_2)) dx \end{aligned} \quad (14)$$

From the derivative of Eq. (14) with a reformulation into Eq. (6), the local extremal optimum is obtained as Eq. (15) with the  $k$  parameter.

$$x_{1,2} = \pm k\sigma \sqrt{\frac{2 \ln k}{k^2 - 1}} \quad (15)$$

As given in Eq. (15) and illustrated in Figure 4 (a), it can be seen that the  $x_{1,2}$  locations are dependent on the  $\sigma$  parameter. While bringing  $x_2 = x_0 + w/2$  the center of the stroke and goes to Eq. (15), we can get the optimum scale  $\sigma_s$  Eq. (16).

$$\sigma_s = \varpi(w) = \frac{w}{2k} \sqrt{\frac{k^2 - 1}{2 \ln k}} \quad (16)$$

As illustrated in Figure 4 (b), two responses  $h_e, h_s$  appear within the model at the  $x_{1,2}$  locations with  $\sigma_s$ .

The response  $h_e$  characterizes the edge of the stroke. It is obtained with Eq. (17) while bringing  $\sigma_s$  Eq. (16) back to Eq. (14), and approximating the Gaussian integral at any location in Eq. (14) with a  $erf(x)$  Gaussian error function  $erf(x) = \frac{2}{\sqrt{\pi}} \int_0^x e^{-t^2} dt$ . For notation simplification, Eq. (17) is given by considering  $x_0 = 0$ .

$$h_e = \frac{a}{2} \left( erf \left( k \sqrt{\frac{\ln k}{k^2 - 1}} \right) - erf \left( \sqrt{\frac{\ln k}{k^2 - 1}} \right) \right) \quad (17)$$

A peak response  $h_s$  appears at the middle of the stroke  $w/2$ . This response decreases while shifting the scaling parameter  $\sigma$  around the  $\sigma_s$  optimum Figure 4 (b). However, no mathematical formulation for  $h_s$  was proposed in the model. This results from the proposed proof that interpolates the stroke response from a step function. At the best of our knowledge, the  $h_s$  formulation has been never investigated in the

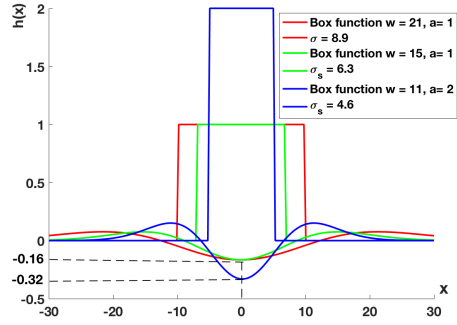


Figure 5: LoG responses at different signal amplitudes and widths of the box function with  $k = \sqrt{2}$ .

literature. Simulation reveals a value  $h_s$  that is independent of the scale parameter  $\sigma$  and proportional to the signal amplitude  $a$ , as illustrated in Figure 5.

The optimization within the scale-space considering the stroke model is attained while applying an optimal quantization  $\sigma_s = \varpi(w)$  of Eq. (16) with  $w \in [w_{min}, w_{max}]$  as a discrete value. The size of the filter bank is then correlated to the stroke width gap of the considered detection problem such as we have  $m = w_{max} - w_{min}$ . With a DoG formulation, this requires  $2(m+1)$  Gaussian kernels for detection.

## 3 PERFORMANCE EVALUATION

### 3.1 Introduction

We present in this section a performance evaluation of the real-time LoG operators with the used dataset, groundtruth and characterization protocol.

Several datasets are available for performance evaluation of text detection such as the ICDAR Robust Reading Competition 2017 and the COCO-text datasets (Gomez et al., 2017; Nayef et al., 2017). These datasets target performance evaluation of text detection where the groundtruth is given at the word level. They are not adapted for characterization of detectors at the pixel level. For this specific purpose, we have developed a semi-automatic groundtruthing process, as given in Figure 6.

This semi-automatic groundtruthing process targets near optimum parameters for scale-invariant LoG filtering. The parameters are fixed with a closed-loop methodology by an expert user, while inspecting the visual quality of the filtered images. The process applied no hand-made modification of the ground-truth, just a control of the parameters. This task uses a prior segmentation of character images. We have applied to a subset of the public Chars74K dataset (de Campos et al., 2009), as presented in Figure 1 and Table

3. This subset has been extracted from full images captured at a low resolution. Our overall process uses four main components  $C_1, C_2, C_3$  and  $C_4$ .

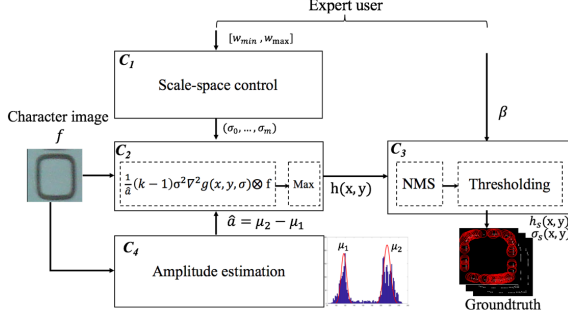


Figure 6: Semi-automatic process for groundtruthing.

- $C_1$  controls the scale-space. For groundtruthing, we applied a brute-force strategy with a filter bank  $\sigma_0, \dots, \sigma_m$  having a large size  $m + 1 = 101$  at regular scale intervals. The minimum and maximum values  $w_{min}, w_{max}$  have been fixed as heuristics by an expert user.
- $C_2$  fixes the operator response. The LoG operator with a normalization  $(k - 1)\sigma^2$  is applied for groundtruthing allowing a direct comparison with the real-time estimators. The responses are computed at all scales and locations, a maximum  $h(x, y)$  is selected.
- $C_3, C_4$  control the response. The selection of a key-point is done with a threshold  $\beta$  fixed by the expert user such as we obtain a key-point if  $h(x, y) > \beta$ . The thresholding is applied after a non-maximum suppression (NMS) step as common for blob detection with the LoG operator (Lindeberg, 1994). As the operator response is dependent on the background/foreground amplitude  $a$ , an estimation  $\hat{a}$  is obtained with the method of (Otsu, 1979) in  $C_4$  and applied for normalization in  $C_2$  before  $C_3$ . For the sake of evaluation, we store for each key-point the optimum response  $h_s(x, y)$  and scale  $\sigma_s(x, y)$ .

Images	7705
Classes	62
Size (Kpixel)	0.3K-10K
$[w_{min}, w_{max}]$	[5, 30]
Resolution of full images	640 x 480 (VGA)

Table 3: The subset of character images in the Chars74K dataset (de Campos et al., 2009).

For characterization, the repeatability criteria is used as a regular metric for local detectors (Rey-Otero et al., 2014a).  $((x_r, y_r, r_r)_{ref}, (x_t, y_t, r_t)_{test})$  are reference and test key-points describing circular regions of

radius  $r_r, r_t$  respectively.  $(x_t, y_t, r_t)_{test}$  is taken under approximation of  $(x_r, y_r, r_r)_{ref}$ . The two regions will be considered as repeated if they respect an overlap error  $\epsilon$  Eq. (18). For the need of evaluation, we have fixed the computation of the radius with the stroke model of Eq. (16), while fixing  $r = w/2$ .

$$1 - \frac{|(x, y, r)_{test} \cap (x, y, r)_{ref}|}{|(x, y, r)_{ref} \cup (x, y, r)_{test}|} \leq \epsilon \quad (18)$$

A global repeatability score indicates how the key-points in the reference feature map are repeated in the test feature map. We denote  $n_r$  and  $n_t$  as the numbers of key-points in the two maps, respectively. The repeatability score is estimated as ratio between number of repeated key-points over minimal of  $(n_r, n_t)$ .

Experimentally, the global repeatability score of a detector is computed as an average of repeatability scores of all character images in the dataset. We relax the value of the parameter  $\epsilon$  to achieve a *ROC-like* curve of the global repeatability score. In most published benchmarks (Rey-Otero et al., 2014a), the parameter  $\epsilon$  is set in range  $[0.3, 1]$  where the value  $\epsilon = 0.4$  is the maximum overlap error tolerated.

The operator responses depend on several aspects as the estimation methods and parameters, the scale-space representation or the signal amplitude. For a detailed analysis, particular characterization tasks must be defined. For this specific purpose, we deployed the architecture of our groundtruthing process Figure 6 and relaxed the components  $C_1$  to  $C_4$ . The Table 4 details our overall protocol.

- The tasks 1 to 4 evaluate the real-time operators.
- The tasks 5, 6 describe the robustness under conditions of low resolution and illumination change.
- The task 7 gives the time processing.

We distinguish these different tasks thereafter.

Task	$C_1$	$C_2$	$k$	$C_3$
Groundtruth	Brute-force	$\frac{1}{a}\sigma^2(k-1)\nabla^2g$	None	$\beta$
Task 1	Brute-force	$\frac{1}{a}(g_1 - g_2)$	$k \in [1, \sqrt{3}]$	$\beta$
Task 2	Brute-force	$\frac{1}{a}(\hat{g}_1 - \hat{g}_2)$	$k \approx 1$	$\beta$
Task 3	Stroke model	$\frac{1}{a}(g_1 - g_2)$	$k \approx 1$	$\beta$
	SIFT			
Task 4	Stroke model	$\frac{1}{a}(\hat{g}_1 - \hat{g}_2)$	$k \approx 1$	$\beta$
Task 5	Stroke model	$\frac{1}{a}(g_1 - g_2)$	$k \approx 1$	$\beta$
Task 6	Brute-force	$(g_1 - g_2)$	$k \approx 1$	$\alpha$
Task 7	SIFT	$g_1 - g_2$	$k \approx 1$	$\alpha$
	Stroke model	$g_1 - g_2$		
	Stroke model	$\hat{g}_1 - \hat{g}_2$		

Table 4: The characterization protocol.

## 3.2 LoG Estimators (Tasks 1, 2)

The characterization tasks 1, 2 are related to the LoG approximation with a DoG and a fast Gaussian filtering method, as discussed in section (2.2). For a fair

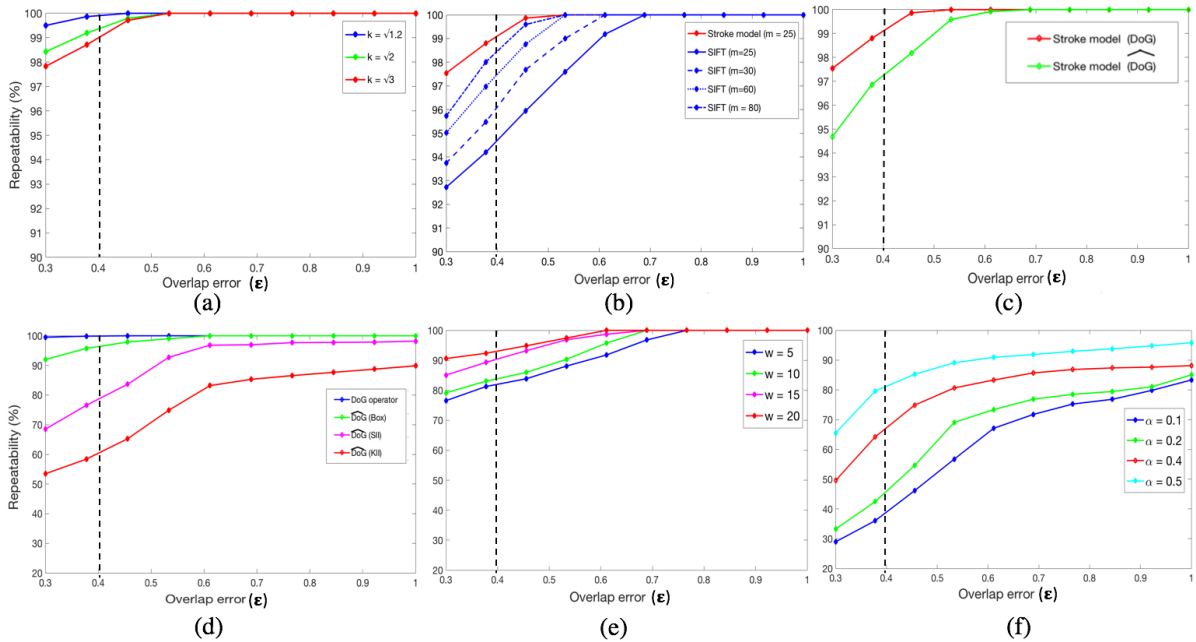


Figure 7: Repeatability score of (a) DoG with different values for the  $k$  parameter (b) the stroke model against the SIFT descriptor (c) the stroke model based on the DoG and  $\widehat{DoG}$  operators (d) DoG estimators based on the Box, SII, KII methods (e) operator responses for low scale characters (f) DoG responses without normalization.

evaluation, we have controlled the scale-space in a brute-force way and applied normalization to the operator response, as done for groundtruthing. By this way, the obtained performances will only characterize the distortion introduced by the LoG approximation.

The results for DoG approximation are given with repeatability as a ROC-like curve Figure 7 (a). The DoG approximation has almost none impact for low  $k \in [1, \sqrt{2}]$ . We observe less than 1% of error in the repeatability score at  $\epsilon = 0.4$ . Distortions start to appear with  $k > \sqrt{3}$ .

To characterize the fast Gaussian filtering, we have selected representative methods for medium, strong and best accuracy in Table 2. The box method has been set with  $n = 5$  and selection of  $\Pi_i(x, y), \lambda_i$  parameters with the method of (Fragoso et al., 2014). In the Figure 7 (d), the methods with a low accuracy introduce several degradations in the detection results, whereas the box method results in less than 5% of repeatability error at  $\epsilon = 0.4$ . The Figure 8 gives a comparison of a detection result among the operators.

### 3.3 Scale-space Representation (Task 3)

At this stage, we compare the SIFT descriptor and the stroke model for the scale-space representation, as presented in section (2.3). We have driven two characterization sub-tasks to compare the representations

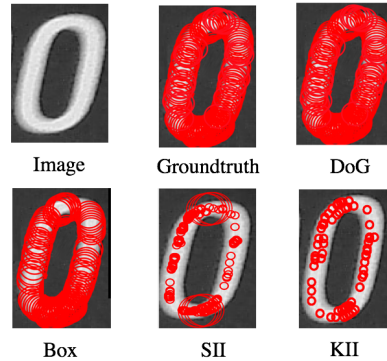


Figure 8: Detection results with different operators.

at a same level of complexity and repeatability.

**Characterization with complexity:** the size  $m + 1$  of the bank filter and the  $\sigma$  parameters are fixed with Eq. (16) of the stroke model using the character widths of the dataset Table 3. Considering  $w \in [5, 30]$ , we have obtained a size of  $m + 1 = 26$  filters with  $\sigma \in [2.3, 14.3]$  requiring 52 Gaussian kernels for a DoG implementation. For a same complexity, we have taken into account a similar number of Gaussian filters for SIFT resulting in 52 scales with the architecture of Figure 3. Taking into account the relation  $\sigma_{max} = k^{2(m+1)} \sigma_{min}$  for the scale-space control within the descriptor, we have achieved  $k = \sqrt{1.06}$ . This value for  $k$  has been applied in the stroke model

too for a similar LoG approximation.

As shown in Figure 7 (b), the stroke model ( $m = 25$ ) with DoG outperforms the SIFT descriptor ( $m = 25$ ) with a gap of 5% repeatability scores at  $\epsilon = 0.4$ . This results of the model and Eq. (16) that guaranties optimum responses of filters at scales  $\sigma_s$  considering a discrete representation of the stroke widths.

**Characterization with repeatability:** in this step we have analyzed the complexity overhead with the SIFT descriptor at a same level of repeatability. Similar to the previous characterization task, we have fixed  $\sigma \in [2.3, 14.3]$  as low and high optimum scale values for detection. We have increased the number of Gaussian filters  $m + 1$  while reducing the  $k$  parameters within the equation  $\sigma_{max} = k^{2(m+1)}\sigma_{min}$  to reach an equal repeatability score with the stroke model. Figure 7 (b) presents the results, where the SIFT descriptor reaches a near-exact approximation (less than 1% of difference between the repeatability scores) at  $m = 80$  for  $\epsilon = 0.4$ .

### 3.4 Real-time Operator (Task 4)

From this task, we have applied a characterization protocol to achieve end-to-end real-time detector. We have set the operator with the stroke model for the scale-space representation, a top accurate method for fast Gaussian filtering with a low value  $k = \sqrt{1.2}$  for an optimum approximation. Figure 7 (c) gives the repeatability scores. This highlights the performance of the detector that has a near-exact approximation of a DoG filter with 2% of error within the repeatability scores at  $\epsilon = 0.4$ .

### 3.5 Low Resolution (Task 5)

As highlighted in the tasks 1 to 4, a closely perfect approximation of the scale-invariant LoG operator can be achieved with a real-time method. A real-time operator is designed to accomplish a near-exact approximation with 2% of error at  $\epsilon = 0.4$ . However, this result is attained from low resolution images ( $640 \times 480$ ) where characters expose from small size  $w_{min} = 5$ .

We analyze here the degradation found by the low resolution. As detailed in section (3.1), our groundtruth is given with a map  $\sigma_s(x, y)$  including the scales  $\sigma_s$  for the optimum responses  $h_s$ . Rather than computing a repeatability score covering all the scales, we have selected the responses at a targeted scale  $\sigma_i$  to get a map  $\sigma_i(x, y)$  Eq. (19). A same process is done for detection.

$$\sigma_i(x, y) = \begin{cases} 1 & \sigma_s(x, y) = \sigma_i \\ 0 & \text{otherwise.} \end{cases} \quad (19)$$

A similar protocol to the task 1 has been applied with  $k = \sqrt{1.2}$  for a strong approximation. By this way, the protocol characterizes the distortion introduced by the low resolution only.

As shown in Figure 7 (e), several degradations emerge for the low scale characters  $w \leq 15$ . This is due to the quantification noise, that produces false detections and miss cases given in Figure 9. As general trend, near to 15% of improvement can be achieved for the repeatability scores while shifting  $w_{min}$  from 5 to 20. Considering the image resolution of the dataset, a recommendation is to shift to a full HD capture to get images at sizes ( $1920 \times 1080$ ) or higher. This will guaranty a robust repeatability at  $w_{min} \approx 20$ .

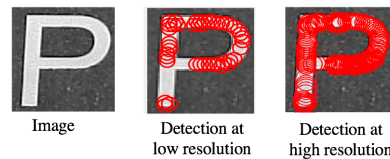


Figure 9: Detection at low and high resolution.

### 3.6 Illumination Change (Task 6)

As discussed in section (3.1) and Figure 6, we have driven our characterization tasks 1 to 5 with a normalization parameter  $1/\hat{a}$  for contrast-invariance. However, within a real-life detection this parameter is unknown. This can result in several degradations of detector performances when important illumination changes appear in the images. Our task 6 clarifies this aspect, where the operator has been applied without normalization. We have used a protocol similar to the task 1 but with a low parameter  $k = \sqrt{1.2}$ . Compared with the previous tasks, we have fixed another thresholding parameter  $\alpha$  taking into account the unnormalized responses.

Figure 7 (f) provides the results where major distortions emerge. For an optimum detection,  $\alpha$  must set high enough to filter out the false positives. In that case the low contrast images raise false negative results and miss detections as depicted in Figure 10.



Figure 10: Detection results without contrast normalization (FD) false detections (MC) miss cases.



This points out the performance limits of the detection due to the illumination changes. This introduces a 20% error as an average in the repeatability score at  $\epsilon = 0.4$ . The design of a contrast-invariant LoG operator is a key topic in the literature as a recent work in (Miao et al., 2016). However, the proposed methods cannot fit with a real-time constraint. As the method of (Miao et al., 2016) is 4 to 5 slower compared to the DoG operator. At the best of our knowledge, real-time and contrast-invariant LoG operators have been never investigated in the literature.

### 3.7 Time Processing (Task 7)

Next to the characterization of detection results, we have evaluated the processing time of the different methods. We have compared the DoG operators described in task 3 with the end-to-end real-time operator of the task 4. This results in three methods given in Table 5. The goal here is to analyze the operators while applying optimization in the spatial and/or scale-space domains. The time processing depends on the complexity of operators and their parameters. As concluded in the tasks 1 to 5, we have fixed

- $n = 5$  for the Gaussian approximation (tasks 1, 2),
- $w \in [5, 30]$  with  $\sigma \in [2.3, 14.3]$  and  $m = 25, 80$  for optimum detection within the scale-space representations at low resolution (task 3),
- image resolutions with the VGA, HD and full HD modes to handle the low resolution (task 5).

Methods	Filter	SS	Comp	VGA (640 × 480)		HD (1280 × 720)		Full HD (1920 × 1080)	
				$m$	$w$	$m$	$w$	$m$	$w$
DoG	Conv	SIFT	$O(N\omega \times m)$	80	[5, 30]	106	[9, 53]	158	[13, 79]
RT-DoG	Conv	SM	$O(N\omega \times m)$	25	[5, 30]	44	[9, 53]	66	[13, 79]
RT-DoG	Box	SM	$O(N \times m)$	25	[5, 30]	44	[9, 53]	66	[13, 79]

Table 5: DoG operators for text detection (RT) real-time (SM) stroke model (Conv) convolution with separability (SS) scale-space (Comp) complexity.

We provide first in Table 6 the numbers of required low-level CPU operations for each of the methods, as done in the literature (Elboher and Werman, 2012). The left part of table gives the formulations with parameters, whereas the right part provides the total amount of operations with the parameter values.

Methods	Parameters (+) + (*)	Number of operations per pixel (in thousands)		
		Use-cases		
		VGA (Char74K)	HD	Full HD
DoG	$2 \sum_{i=0}^m (2\omega_i + 2\omega_i)$	25.89K	61.02K	133.57K
RT-DoG	$2 \sum_{i=0}^m (2\omega_i + 2\omega_i)$	10.3K	31.8K	70.4K
RT-DoG	$2(m+1)(4n+n)$	1.3K	2.25K	3.35K

Table 6: Arithmetic operations per pixel for the operators.

We acquire one to two orders of magnitude of execution time with optimization in the spatial and scale-

space domains, where one order is obtained with the fast Gaussian filtering method. The complexity of operators are  $O(N\omega)$ ,  $O(N)$  respectively, the RT-DoG operator performs well as the image resolution raises.

The Table 7 gives the processing times. All the methods have been implemented at a same level of parallelism for a fair comparison with a single thread and auto-vectorization (Mitra et al., 2013). These results fit with the parameters given in Table 6 considering the additional time to get the integral image for the RT-DoG operator and the difference between the pipelines for vectorization.

With multithreading, the operators can support a regular frame rate even with a HD, full HD capture. Let's note that a near time 3 acceleration factor could be acquired for all the methods, while applying hand optimized intrinsic functions (Mitra et al., 2013). However, this approach makes the code CPU dependent that raises portability constraints. The overall complexity could be shifted to a sublinear level with spatial and scale-space sampling (Lowe, 2004; Rey-Otero et al., 2014b), that introduces other degradations and constraints.

Methods		DoG	RT-DoG	RT-DoG
Threads		1	1	1
Processing time (ms)	VGA	988	437	164
	HD	8058	4135	857
	Full HD	42170	21630	3190

Table 7: Time processing of operators in (ms) performing with the C++ on a Mac- OS 2.2 GHz Intel Core i7 system.

## 4 CONCLUSIONS

The real-time LoG operators with one to two orders of magnitude of execution time are given. Adaptation to text detection is attained through the scale-space representation. They can support for modern camera devices because of their ability to perform efficiently with high resolution images.

As perspectives, the real-time operators are not robust to illumination changes. This is a crucial problem for text detection, real-time methodologies for contrast-invariance should be investigated (Miao et al., 2016). Additional optimization could be proposed with sampling in the spatial and scale-space domains. This requires specific models linked to detection problems (Rey-Otero et al., 2014b).

This work gives a performance evaluation at the detector level. The characterization for full text detection must be addressed, for an objective comparison with other real-time detectors.

A further issue is to characterize the two-stage and end-to-end strategy. Real-time operators target a perfect recall for detection for search-space reduction.

They can result in a large optimization when used as input of a template/feature matching method. Indeed, such a method requires GPU support and low resolution images to fit with a real-time constraint (Liao et al., 2017).

## REFERENCES

- Bhatia, A., Snyder, W., and Bilbro, G. (2010). Stacked integral image. In *International Conference on Robotics and Automation (ICRA)*. 1530–1535.
- Charalampidis, D. (2016). Recursive implementation of the gaussian filter using truncated cosine functions. In *Transactions on Signal Processing (TSP)*. 64(14):3554–3565.
- de Campos, T., Babu, B., and Varma, M. (2009). Character recognition in natural images. In *International Conference on Computer Vision Theory and Applications (VISAPP)*.
- Deshpande, S. and Shriram, R. (2016). Real time text detection and recognition on hand held objects to assist blind people. In *International Conference on Automatic Control and Dynamic Optimization Techniques (ICADOT)*. 1020–1024.
- Elboher, E. and Werman, M. (2012). Efficient and accurate gaussian image filtering using running sums. In *International Conference on Intelligent Systems Design and Applications (ISDA)*, 897–902.
- Fragoso, V., Srivastava, G., Nagar, A., and Li, Z. (2014). Cascade of box (cabox) filters for optimal scale space approximation. In *Conference on Computer Vision and Pattern Recognition Workshops (CVPRW)*. 126–131.
- Girones, X. and Julia, C. (2017). Real-time text localization in natural scene images using a linear spatial filter. In *International Conference on Document Analysis and Recognition (ICDAR)*. 1:1261–1268.
- Gomez, L. and Karatzas, D. (2014). Mser-based real-time text detection and tracking. In *International Conference on Pattern Recognition (ICPR)*. 3110–3115.
- Gomez, R., Shi, B., Gomez, L., Numann, L., and Veit, A. (2017). Icdar2017 robust reading challenge on coco-text. In *International Conference on Document Analysis and Recognition (ICDAR)*. 1435–1443.
- Gonzalez, R. and Woods, R. (2007). Image processing.
- Kong, H., Akakin, H., and Sarma, S. (2013). A generalized laplacian of gaussian filter for blob detection and its applications. In *Transactions on cybernetics*. 43(6):1719–1733.
- Kovesi, P. (2010). Fast almost-gaussian filtering. In *International Conference on Digital Image Computing: Techniques and Applications (DICTA)*. 121–125.
- Liao, M., Shi, B., Bai, X., Wang, X., and Liu, W. (2017). Textboxes: A fast text detector with a single deep neural network. In *AAAI*, 4161–4167.
- Lindeberg, T. (1994). Scale-space theory: A basic tool for analysing structures at different scales. In *Journal of Applied Statistics*. 21.224–270.
- Liu, Y., Zhang, D., Zhang, Y., and Lin, S. (2014). Real-time scene text detection based on stroke model. In *International Conference on Pattern Recognition (ICPR)*. 3116–3120.
- Lowe, D. (2004). Distinctive image features from scale-invariant keypoints. In *International Journal of Computer Vision (IJCV)*. 60(2):91–110.
- Mao, J., Li, H., Zhou, W., Yan, S., and Tian, Q. (2013). Scale based region growing for scene text detection. In *International Conference on Multimedia Retrieval (ICMR)*. 1007–1016.
- Miao, Z., Jiang, X., and Yap, K. (2016). Contrast invariant interest point detection by zero-norm log filter. In *Transactions on Image Processing (TIP)*. 25.(1):331–342.
- Mitra, G., Johnston, B., and Rendell, A. (2013). Use of simd vector operations to accelerate application code performance on low-powered arm and intel platforms. In *International Symposium on Parallel & Distributed Processing, Workshops (IPDPSW)*. 1107–1116.
- Nayef, N., Yin, F., Bizid, I., Choi, H., and Feng, Y. (2017). Icdar2017 robust reading challenge on multi-lingual scene text detection and script identification-rrc-mlt. In *International Conference on Document Analysis and Recognition (ICDAR)*. 1:1454–1459.
- Neumann, L. and Matas, J. (2016). Real-time lexicon-free scene text localization and recognition. In *Transactions on Pattern Analysis and Machine Intelligence (PAMI)*. 38(9):1872–1885.
- Nilufar, S., Ray, N., and Zhang, H. (2012). Object detection with dog scale-space: a multiple kernel learning approach. In *Transaction on Image Processing (TIP)*. 21(8):3744–3756.
- Otsu, N. (1979). A threshold selection method from gray-level histograms. *IEEE*, 9(1): 62–66.
- Rey-Otero, I., Delbracio, M., and Morel, J. (2014a). Comparing feature detectors: A bias in the repeatability criteria, and how to correct it. arXiv:1409.2465.
- Rey-Otero, I., Morel, J., and Del, M. (2014b). An analysis of scale-space sampling in sift. In *International Conference on Image Processing (ICIP)*. 4847–4851.
- Risnumawan, A., Shivakumara, P., and Chan, C. (2014). A robust arbitrary text detection system for natural scene images. In *Expert Systems with Applications*. 41.18:8027–8048.
- Salahat, E. and Qasaimeh, M. (2017). Recent advances in features extraction and description algorithms: A comprehensive survey. In *International Conference on Industrial Technology (ICIT)*. 1059–1063.
- Yang, H., Wang, C., Che, X., Luo, S., and Meinel, C. (2015). An improved system for real-time scene text recognition. In *International Conference on Multimedia Retrieval (ICMR)*. 657–660.
- Ye, Q. and Doermann, D. (2015). Text detection and recognition in imagery: A survey. In *Transactions on Pattern Analysis and Machine Intelligence (PAMI)*. 37.7: 1480–1500.